

# A Multi-Channel Electrode for Chronic Recording and Safe Current-Steered Stimulation

Ben Pearre<sup>1,a,✉</sup>, Sanne Moorman<sup>1,b</sup>, Jun Shen<sup>1,c</sup>, Stuart F. Cogan<sup>2,d</sup> Timothy J. Gardner<sup>1,e</sup>

<sup>1</sup> Department of Biology, Boston University, Boston, Massachusetts, United States of America

<sup>2</sup> Department of Bioengineering, University of Texas, Dallas, Texas, United States of America

Author <sup>a</sup> did something, we think. The histology data analysis was by Author <sup>b</sup>. Author <sup>c</sup> performed all surgeries. Authors <sup>b</sup> and <sup>c</sup> did the histologies. Author <sup>d</sup> developed the iridium oxide coating technique. Author <sup>e</sup>, the PI, designed and guided the experiment and this paper.

✉ Corresponding author: bwpearre@gmail.com (BP)

## Abstract

Electrical control of the brain facilitates a variety of therapeutic and scientific goals, from treating sensory, motor, and cognitive defects to exploring the effects of disrupting or subtly modifying the brain's behaviour in real time. These procedures are limited by the brain's reaction to foreign matter: over a period of months, glia encapsulate the electrodes, isolating them from neurons, allowing monitoring and control of the brain only over large spatial scales—often on the order of hundreds of microns. Small electrodes ( $< 10 \mu\text{m}$ ) minimise encapsulation, and thus can both record single neurons for many months and precisely stimulate small groups of neurons. However, the high impedance of small electrodes can require stimulation voltages that exceed the water hydrolysis point.

We have developed an electrode design in which groups of thin electrodes support each other during insertion and then splay in the brain, minimising

damage and encapsulation, and thus allowing long-term small-spatial-scale recording and stimulation.

We describe the splaying properties of these electrode arrays in the brain. We present preliminary results showing that these electrodes remain capable of recording individual spikes for a year after implantation, even when also used to stimulate.

We present preliminary evidence that the spatial scale of the splaying is sufficient to allow the steering of current between the electrodes, and that this allows a degree of high-dimensional control over the brain's response to stimulation. We show that appropriate control of the electrode array can produce neural responses while keeping stimulation voltages below safety limits. Furthermore, we demonstrate controllable differentiation between responses, even when measured in a brain area upstream of the stimulation site.

Thus these multichannel, spatially distributed, micron-scale arrays allow long-term single-unit recordings, enabling new experiments investigating how the brain changes on long timescales. In addition, current-steered control of stimulation inputs allows fine-grained control over small groups of neurons, potentially permitting a wide variety of optimisations, such as controlling the brain to some set of desired responses, or minimising the voltage or energy required in order to achieve a desired result.

## 1 Introduction

Goal: controlling the brain.

How it's done now: large electrodes, coarse stimuli, crude if any feedback control (due to large electrodes), poor control due to imprecision of stimulation.

How we want to do it: small electrodes that splay.

- Small size permits chronic single-unit recording, but delicate.
- Bundled, they are strong enough to implant.
- Current steering may overcome stimulation current and voltage restrictions.
- Small size, splayed geometry, high channel count allow a new frontier in fine-grained control.

## 1.1 Review of electrode size and damage

*Large electrodes must be stimulated at high currents. Energy inefficiency. Imprecision. Sense-act cycles are limited.*

Electrodes with cross-sectional dimension above about 10  $\mu\text{m}$  cause tissue damage during surgery as well as glial encapsulation over time. For example, [1] assumes a 500- $\mu\text{m}$  encapsulation layer for the  $\sim 1.3\text{-mm}$  electrodes common in DBS. This encapsulation results in ever-increasing stimulation thresholds, rendering the electrodes unable to record as effectively [2–5].

This is mitigated by electrodes  $< 10 \mu\text{m}$ , but these present two difficulties: they are too weak to insert, and during stimulation, their small surface area requires high voltage in order to deliver sufficient current to induce response.

Our hexadecode [6] uses multiple shanks each of which is too small to stimulate adverse tissue reactions. The shanks are bundled to support each other during insertion. They splay in the brain, giving randomly distributed sites for recording and stimulation.

**Charge injection** In order to increase the charge injection capacity of our electrodes, we tried electroplating them with iridium oxide. This effected an improvement of roughly an order of magnitude: impedances went from around 2 M $\Omega$  to 200 k $\Omega$ , and for a given current, the required voltage was much lower. We also experimented with PEDOT, which has excellent charge-injection properties, but we found it to have durability issues. See [7] for a review of electrode physics.

## 1.2 Review of current steering

**Deep Brain Stimulation** Much of the work in current steering in the brain is due to the interest in deep brain stimulation (DBS). Electrodes tend to be single rods 1.2–1.6 mm in diameter with 4–32 contacts.

DBS has been used to treat movement disorders (especially those associated with Parkinson’s disease), epilepsy, Alzheimer’s, chronic pain, cluster headache, depression, OCD, addictive behaviours, anorexia. . .

Most attempts to steer current use computational models of brain tissue to predict

FIXME

All I know about this is hearsay.

Many more! But do we want to provide a big list? Only if we are selling this as a clinical paper, right?

Review what’s known of DBS’s mechanisms of action? Perhaps only marginally relevant, but there’s a good review in [8].

current-steering configurations that preferentially target the intended type of tissue, or  
make up for errors in electrode placement during surgery [9]. One approach [1, 10]  
builds a model of the tissue of interest using magnetic resonance imaging (MRI) and  
diffusion tensor imaging (DTI) [11, 12], which produces data with voxels of roughly 2  
mm<sup>3</sup>. They then use 3D finite element analysis to predict current steering trajectory.

Lots more references might be added here, all of which have spatial resolution on this order and a variety of temporal resolutions; choose  $\approx 3$  or just cite a review?

Current-steered and adaptive DBS have been shown

**Current steering on a smaller scale:** [13] use 64-channel electrode arrays, with  
electrode as closely packed as 30  $\mu\text{m}$ , to stimulate macaque retina *in vitro*. They  
stimulated the retina using single electrodes or combinations of three electrodes with  
charge-balanced pulses, and found that retinal response could be predicted with a  
piecewise linear model.

Note about how different retina structure is from our areas?

**Something?** Efforts to steer current outside of the brain have also been  
pursued, [14] describes an algorithm for clinician-assisted search for effective  
stimulation in multielectrode arrays in the spinal cord. The patent defines an  
algorithm for hillclimbing search, controlled by a clinician. [15] develops an even more  
creative specialised hillclimbing search method. However, we have not seen application  
of standard optimisation techniques in this domain.

Sounds so weak! Turn this into a bigger review?

### 1.3 Stimulation: closing the loop

Standard DBS systems deliver some kind of stimulation continuously. Recently,  
interest in using biological feedback has grown. Due to the size of the electrodes, for  
feedback control most systems rely on large-spatial-scale metrics such as local field  
potentials (LFP) [16] and other macroscopic measures of outcome such as surface  
electromyography and accelerations [17] but the addition of a second electrode in a  
different brain region has been shown to be effective in ameliorating Parkinsonian  
symptoms in monkeys [19].

Basu, "Pathological tremor prediction using surface electromyogram and acceleration"

Great review: [18]

## 1.4 Contribution

# 2 Materials and Methods

## 2.1 Bird surgery description

**Animals and Perfusions** At the end of the experiment, the birds were given an overdose of pentobarbital and perfused with 0.1M phosphate buffer followed by 4% paraformaldehyde in 0.1 M PB. Brain with skull were removed. The electrodes were secured on the skull and brain. 2–4 holes were made on the skull to facilitate the solutions to get in. Following an overnight postfix in 4% paraformaldehyde, brain with skull was treated overnight in 15% and 30% sucrose in 0.1M PB at 4°C. The brain slice with the electrodes were collected. The tissue samples were sectioned toward to the tips of the implanted electrodes at 50–100μm by a cryostat (CM 3050 S, Leica). The tissue samples were stored in –20°C until immunohistochemistry was processed.

**Fluorescent Immunohistochemistry of NeuN, MBP and DAPI** Sections of the brain were used for immunohistochemical staining of Neun and DAPI. Non protein binding was blocked with 5% normal donkey serum. The primary antibody against neuronal nuclei was a mouse anti-NeuN antibody (1:500, MAB377, A60, Chemicon) and the primary antibody against myelin was a rabbit Anti-Myelin Basic Protein / MBP Antibody (1:500, LS-C312288, LifeSpan BioSciences, Inc). Following primary antibodies incubation for overnight at 4°C, Alexa Fluor® 488 AffiniPure Donkey Anti-Mouse IgG (H+L) (1:500, 715-545-150, Jackson ImmunoResearch Laboratories) and Rhodamine (TRITC) AffiniPure Donkey Anti-Rabbit IgG (H+L) (1:500, 711-025-152, Jackson ImmunoResearch Laboratories) added. The sections were coated with mounting medium containing 4',6-diamidino-2-phenylindole (DAPI, VECTASHIELD). The sections of brain were visualized and the images were captured using a FV10i confocal microscopy(Olympus) and Olympus FV10i software.

**Surgery information** All procedures were approved by the Institutional Animal Care and Use Committee of Boston University (protocol number 14-029). Zebra finches (n = ?; ?for acute experiments, ? for chronic HVC and Area X recordings and

Jun?

? for histology) (>120 days post-hatch) were anesthetized with 4.0% isoflurane and maintained at 1–2% isoflurane during the aseptic surgical procedure. The analgesic Meloxicam (4mg/kg) was injected intramuscularly into the breast at the start of the procedure and the animal was placed into a stereotaxic instrument. Feathers were removed from the scalp and a Betadine solution applied. Bupivacane (4mg/kg) was then injected subcutaneously into the scalp before an incision was made along the AP axis.

The same surgical procedure was followed for the acute and chronic recording in Area X and HVC [6]. The skull over area X was localized using stereotactic coordinates (20° head angle; 5.8 mm AP, 1.5 mm ML, 2.8 mm DV) and the skull over HVC was localized using stereotactic coordinates (30° head angle; 0.7 mm AP, 2.3 mm ML, 0.4–0.7 mm DV), and the the outer bone leaflet removed at the location of area X and HVC with a dental drill. The lower bone leaflet was carefully removed with an orbital scalpel, similar to implant procedures for recording with microdrives [20], exposing a hole of  $\sim 150\mu\text{m}$  diameter. A minimal durotomy was performed using a dura pick (typical durotomy was less than 50 microns.). A 16-channel carbon-fibre array [6] was mounted on a digital manipulator attached to the stereotax and slowly lowered through the durotomy. During insertion into the brain, the carbon fibres would occasionally begin to visibly splay. After lowering the array to the appropriate depth, the position in the song nucleus HVC was verified using antidromic stimulation from another 16-channel array implanted in downstream Area X [6,21]. After verifying the position of the array, the craniotomy was covered with the silicone elastomer Kwik-Sil (World Precision Instruments), and the array was glued into place using light-bonded acrylic (Flow-It ALC, Pentron) along the entire length of the electrode shank, such that no portion of the carbon fibre bundle was left exposed or loose. A  $\sim 150\mu\text{m}$  hole was made on the skull of cerebellum and both arrays' grounding wires were secured in cerebellum using light-bonded acrylic.

## 2.2 Electrode construction

Electrode arrays were constructed as described in [6]. The charge transfer capacity of one of the electrode arrays used for stimulating in Area X was enhanced by

electrodeposited iridium oxide. [7] describes the electrochemistry of charge transfer. 123

## 2.3 Splay histology 124

Electrode bundles were implanted into birds, all to a depth of roughly 3 mm. Most of these were “dummy” uncoated and blunt-cut rather than fire-sharpened as in [6], with 10–16 channels (fibres). The birds were killed, and their brains sectioned roughly perpendicularly to the electrodes, with a slice thickness of 50  $\mu\text{m}$ . 125  
126  
127

Sanne: what slice thickness?

The following criteria were used to exclude observations: 128  
129

- Individual fibres were excluded if they were lying flat on the surface of the tissue (visible as side-on cylinders). 130  
131
- Bundles were excluded if they were implanted in fibres of passage. 132

Clustering was done by hand. The set of distances between electrodes was computed by measuring the distance between each electrode and its nearest neighbour. Bundles were clustered as follows: 133  
134  
135

I'm about a day from finishing software to do all-to-all comparison. For the draft (and possibly first submission, if time is tight) this suffices.

**Splayed:** All electrodes were more than 10  $\mu\text{m}$  from each other, or at most one pair was closer. 136  
137

Why 10  $\mu\text{m}$ ?

**Partial:** Some electrodes were more than 10  $\mu\text{m}$  from each other. 138

How many?

**Clumped:** All electrodes were within 10  $\mu\text{m}$  of each other. 139

All-to-all, or nearest-neighbour?

Examples of these three categories are shown in Fig. 1. 140

Would it make sense to automatically cluster the splay data? Or to change the criteria? I can think of some changes...

## 2.4 Recording 141

For electrophysiology (recording and stimulation), birds were anaesthetised with 1.5% isoflurane, 98.5% oxygen, at 0.5 liters/minute. 142  
143

Recording of spontaneous activity in Area X was with an Intan RHD2000 amplifier at 20 kHz, with a hardware high-pass filter at 200 Hz. 144  
145

## 2.5 Stimulation: Zebra finch antidromic HVC $\leftarrow$ X 146

A common technique for locating HVC in the zebra finch involves implanting a stimulating electrode in Area X and looking for a an antidromic response [21,22], 147  
148

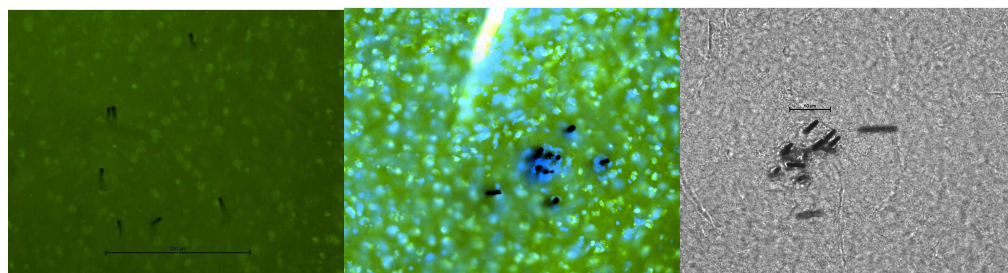


**Figure 1.** Splay types, left to right: examples of full splay, partial splay, and clumped. In all images, black circles are electrode shafts; in many cases the slicing plane is not quite orthogonal to the electrodes, yielding oblong images. In the bright-field image on the right, three of the electrode slices were pulled out of the tissue during slicing, and appear to lie flat on the slide. Since their original locations cannot be determined, we have ignored them.

which is visible in HVC but not in the surrounding tissue.

Electrical stimulation saturates the brain, including the recording electrode, for some time post-stimulation (depending on the hardware used, but generally 1–3 ms post-stimulation). Responses to stimulation can be detected outside of that saturation window.

We tested our ability to steer current in the brain by stimulating in Area X and monitoring the response in HVC, about 5 mm away. This spatial separation results in synaptic transmission delays of between 3 and 8 ms, which gives the recording amplifier time to settle before measuring the response.

We will use the following definitions:

**Channel:** Our electrodes have 16 separate carbon fibres, each one of which we consider a separate channel, since each is connected to a separate amplifier.

Some work better than others, and usually about 75% of them have low enough impedance to use. We refer to these as active channels, or just channels.

**Pulse:** A biphasic charge-balanced square wave of current. Each phase is 200  $\mu$ s long, and there is no interpulse interval.

**Current-steering configuration (CSC):** The configuration defining which channels receive the positive half of their biphasic pulse first, or vice versa.

**Pulse train:** A sequence of 10 identical pulses delivered simultaneously to all active

Tim: citation for 3–8 ms?

But why antidromic?



channels at 25 Hz. This is slow enough that pulses do not interfere with each other, and is used to detect the reliability of the response.

Move timing notes to Discussion of compromises required for this experiment?

- Programming the Plexon stimulator for one pulse train requires about 2 seconds.

**Threshold scan:** A series of pulse trains, each of which has the same CSC but a different current, designed to find the minimum current for this CSC that will antidromically induce a response in HVC. The algorithm is described below.

- A threshold scan generally requires roughly 15 pulse trains, and thus takes on the order of 30 seconds.

**Voltage scan:** The Plexon hardware can deliver a current-controlled pulse to each of 16 channels independently, but only allows monitoring of the voltage delivered on one channel at a time. A voltage scan involves sending the same pulse train once per active electrode, monitoring a different one each time.

This does not require full reprogramming of the Plexon! Just setting the monitor channel is faster, but my code does not take advantage of this, and fully reprogrammes the Plexon each time.

- A voltage scan requires delivering one pulse train per active electrode, taking a total of about 30 seconds.

Jun?

The stimulation and recording electrodes use separate electrical returns, consisting of silver wire in contact with the skull. Some CSCs balance current delivery between the electrodes, whereas others do not, and in the latter case excess current flows through the common return.

And/or an Intan, depending on which recording to show in Fig. 2

We used a Plexon stimulator to control stimulation in Area X, and recorded from HVC using a Tucker-Davis Technologies (TDT) RZ5 amplifier. The Plexon self-monitoring channels were recorded on a National Instruments (NI) PCI-6251 data acquisition card using the session-based interface of Matlab (various versions from 2014a through 2015b) on Windows 8.1.

Custom MATLAB software controls the experiment, initiating spike train delivery and response monitoring. The Plexon's self-monitoring channels are recorded by the NI card, and the neural response in HVC is recorded by the TDT. In order to guarantee precise temporal alignment between stimulus delivery and response measurement, all hardware is triggered by a TTL pulse from the NI card when it

begins its acquisition cycle. The Plexon begins stimulating upon receipt of that TTL pulse, and the TDT begins recording at 24.414 kHz (the device's native frequency) on the same signal. Whenever the Plexon is actively delivering current (i.e. during each pulse within the train) it sends out its own TTL pulse: this signal is recorded by the TDT along with the HVC electrode voltages. Thus the data alignment precision is controlled by the sampling rate of the TDT (41  $\mu$ s).

**Response detection** HVC projects into Area X (and into RA, which we do not discuss here). When Area X is stimulated, an antidromic response may be observed both in HVC<sub>X</sub> projection neurons and in HVC interneurons. The antidromic response occurs roughly 3–8 ms after the stimulation pulse, and is highly stereotyped: [23] reports that the variability in the timing of the antidromic response in HVC<sub>X</sub> projection neurons is under 50  $\mu$ s, while that of HVC interneurons is above 500  $\mu$ s.

Fig. 2 shows an example of a pronounced HVC response to stimulation in Area X. In order to detect this signal, we measure the cross-correlation between the recorded response for each pulse in a train and each other with a maximum lag of 50  $\mu$ s, which provides a robust way of separating neural response from noise. Because the HVC amplifier's (Intan's or TDT's) response to the transient stimulation pulse in Area X can persist into the time of interest (3–8 ms), each response is first de-trended using a maximum-likelihood fit over the region 2–25 ms using an eighth order Fourier Series, which removes post-stimulation decay while leaving intact spike-sized signals. We found this strongly biased smoothing technique to produce fewer artifacts than the more conventional approach of bandpass-filtering the signal, given the large stimulation artifact. The cross-correlation threshold above which a response is identified is chosen by visual inspection.

As the bird ages, the implant bonding site is slowly pushed away from the skull. For shallow installations such as HVC (depth  $\approx$  200  $\mu$ m, the quality of the HVC recordings diminishes as electrodes are forced out of contact with the brain. This makes it more and more difficult over time to measure the antidromic response. The above cross-correlation technique is more sensitive than the technique typical of acute or short-term response measurements, in which a pronounced spike is often clearly visible. We are confident that we are measuring an antidromic response because it is

Citation!

Filtering would probably work better with the TDT than with the Intan...

But now why not findpeaks  $3\sigma$  or whatever, and see if peak jitter is  $< 50\mu$ s as required by [23]? This has the great advantage that over an  $n$ -spike train, I could immediately compute  $\Pr(\text{response})$  (see marginpar QWE to see why this is a good idea). I reanalysed the old data this way and compared... see below.

Details or citation? Possibly [2], although they don't really discuss this so much.

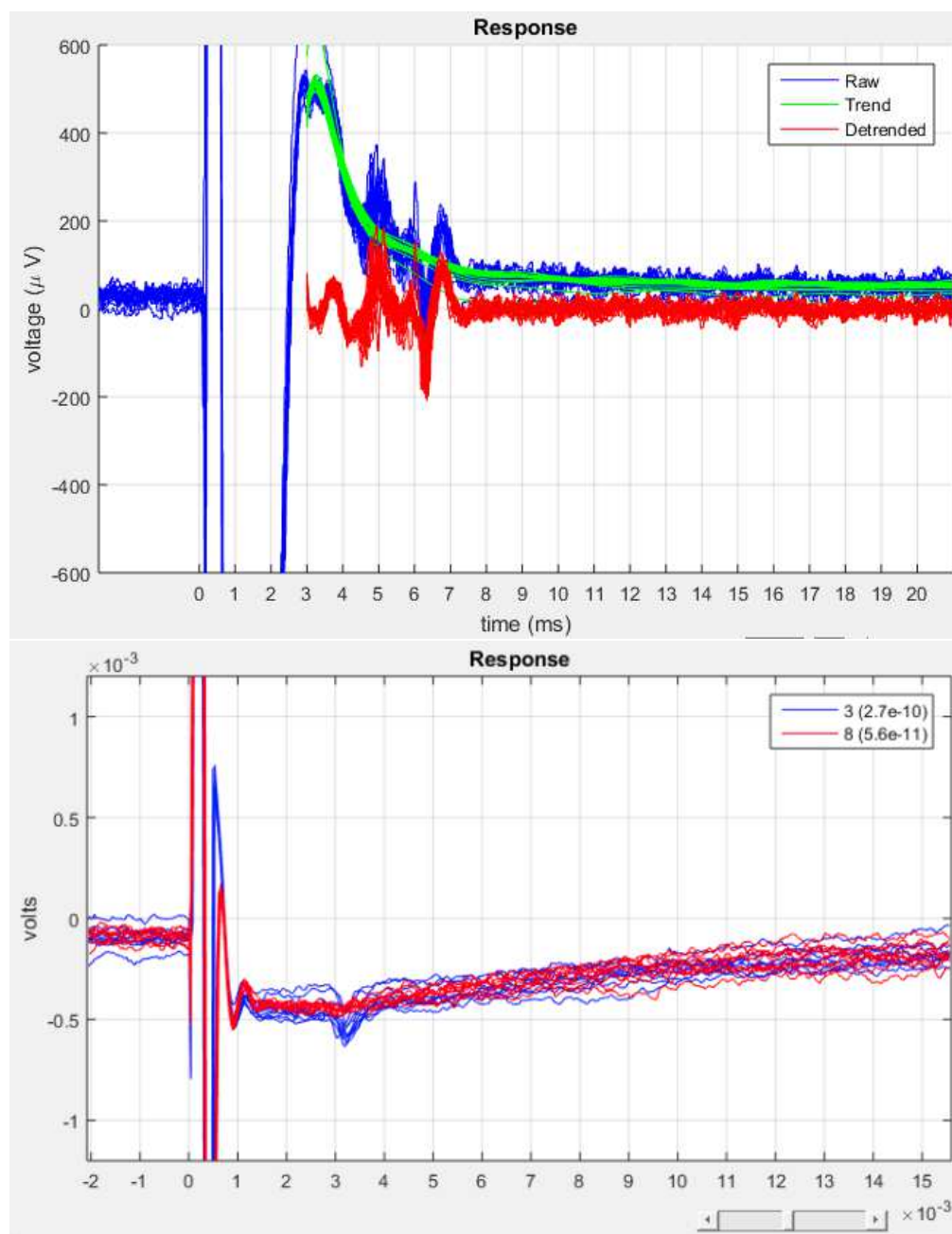


**Figure 2.** An example of a strong response in HVC. **Top:** The horizontal axis is time in milliseconds relative to the onset of a stimulation pulse. Here, the stimulation is a 400- $\mu$ s biphasic pulse of 3  $\mu$ A, in which voltage peaked at 1.6 V. Stimulation was repeated 20 times at 25 Hz, with each response aligned to its respective pulse. Various response activity can be seen, but the most pronounced is at 6.2 ms post-onset. **Bottom:** a different bird, with a much weaker signal, but recorded on TDT. 200  $\mu$ s, 6.94  $\mu$ A, 1.2 V peak. Use the top figure? It only shows one channel, and it's recorded on the Intan, which I was using while the HVC signals were still pretty. That means a lot worse amplifier settling, so it's not the best image, but the response is much cleaner than later ones made with the TDT.

Cite papers giving timing and stimulation threshold.

How can we establish how much robustness to noise is required?

Perhaps write a pseudocode block instead of this mess?

Search could even be conducted as above (although could do better) or terminated by estimating the error on the estimate.

on the correct timescale and appears near the expected stimulation threshold.

**Threshold scan** What stimulation parameters are required in order to reliably elicit an antidromic response to stimulation in Area X? How can this threshold be found quickly, while minimising the risk of exceeding safe stimulation voltages? How can this process be made robust to noise?

After choosing a CSC, we begin stimulating at a current that is known to be below threshold. While no response is seen, the current is increased gradually (by a factor of  $\alpha \approx 1.1$ ) until either a response is detected or the voltage or current limit is exceeded. In the latter case, a lack of response is reported, and we move on to the next CSC. If a response is found, then the step size is decreased towards unity ( $\alpha \leftarrow \alpha^{2/3}$ ) and we reduce the current until the response disappears. This process is repeated until the step size drops below a limit ( $\alpha < 1.02$ ), and the threshold is taken as the last parameter set that induced a response.

A further, independent response-detection analysis was performed on the data set: for each train of  $n$  pulses, we labeled peaks greater than 5 standard deviations from the RMS noise of a nearby (within 20 ms) non-stimulated recording on the same electrode. For each of the  $n$  stimuli in the train, all peaks' delays post-stimulus were compared to those from the other  $n - 1$  responses, and any peak whose delay was within 100  $\mu$ s of another peak was considered a response to the stimulus. The probability of a response at this current was then the maximum number of aligned peaks divided by the number  $n$  of pulses in the train. Given the set of points  $\text{Pr}(\text{response} \mid \text{maximum electrode voltage})$ , we then fit a sigmoid  $0.5 + 0.5 \tanh(\lambda(x - \mu))$  to this curve, and take the midpoint  $\mu$  as an alternative measure of the voltage required to induce a response with probability 50%.

While a larger step size would result in a faster search, and a binary search would be easier to describe, this ad-hoc approach samples near the current of interest while making it unlikely that we will stimulate with a current that significantly exceeds the minimum required for a response, and thus minimises the possibility of injuring the bird.

# Good electrodes	Inter-electrode distance ( $\mu\text{m}$ )		
	Mean	StdDev	Max
3	5.0	0	20.0
10	6.0	2.1	52.9
16	6.3	6.3	48.3
4	7.5	5.0	35.8
6	16.7	18.9	44.8
9	7.7	5.5	107
14	12.8	12.1	15.2
8	14.7	17.8	108
15	15.1	10.2	163
15	19.3	19.1	128
5	22.0	27.7	103
9	28.2	35.8	148
11	31.8	28.1	103
8	35.9	30.6	228
13	76.5	152	167
5	51.4	28.1	51.5
3	20.0	0	123
6	73.5	35.5	128
8	38.5	35.2	142
9	47.4	31.5	208
5	126	63.5	214
16	62.0	58.9	829

**Table 1.** Raw data. Each row shows the statistics from one electrode array. “Good” electrodes is the the number of carbon fibre electrodes in each bundle that appeared to still be firmly fixed in the neural tissue after slicing.

**Voltage scan** Once the minimum current required in order to achieve a response is identified, we perform a voltage scan at that current, in order to measure the peak voltage delivered to each electrode.

### 3 Results

#### 3.1 Splay histology

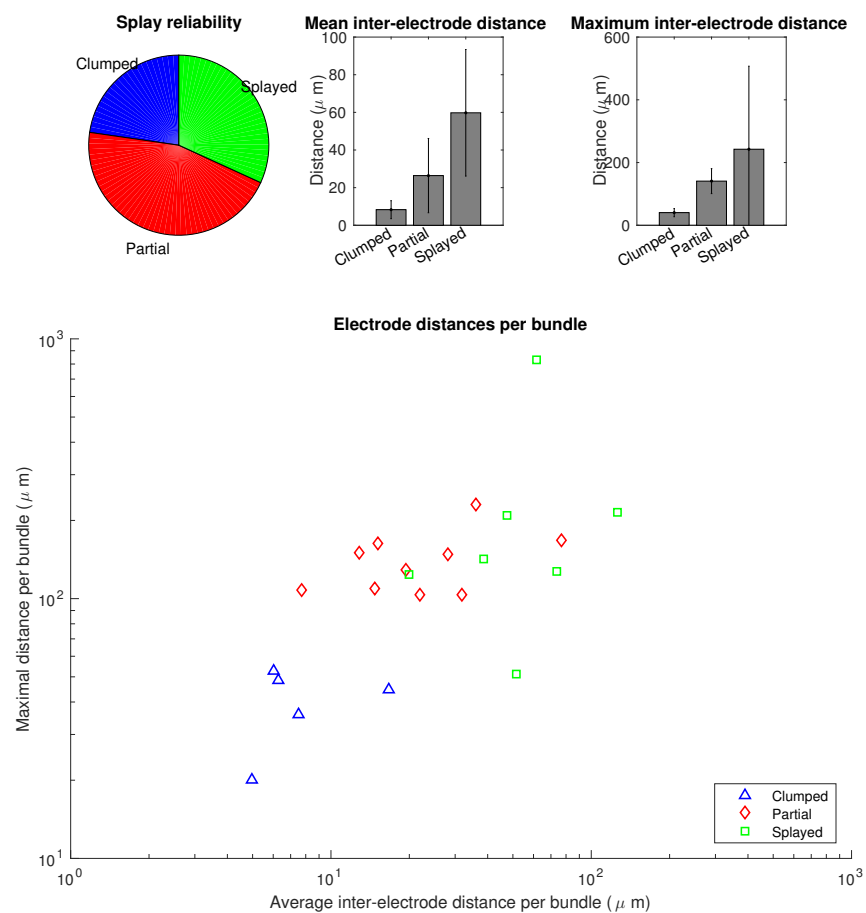
After exclusion, 22 arrays, implanted into 13 different birds, each yielded at least 3 measurable electrodes. See Table 1 for the raw data and Fig. 3 for visualisations thereof.

Fig. 4 shows some examples of the damage done to the brain in the vicinity of tle electrodes. Visual inspection shows little damage in the vicinity of single electrodes, and slightly more in clumped electrode groups. Visual inspection can give some indication of the damage done to the brain and the likelihood of achieving good

Perhaps take out the table and just use the graphs?

An image of “typical” damage done by “micro”electrodes would be nice, but it’s hard to show what’s typical of the competition prior work with any credibility. Letting people compare vs. their own experiences is the best, but not everyone (e.g. me) will know what’s typical.

I have data on how long post-implant the birds lived, which needs to come along with this figure, if not the rest of the paper.



**Figure 3.** Splay histology data from Table 1.

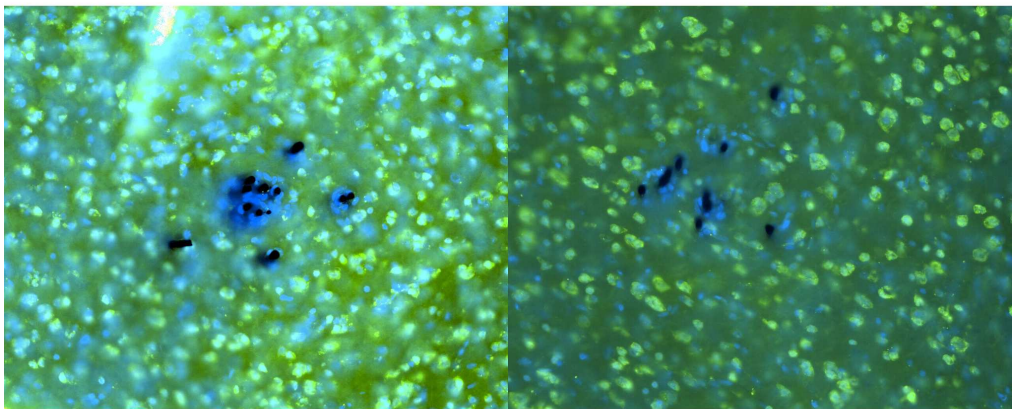


**Figure 4.** Damage. Neural nuclei are shown in green (stained with NeuN) and all cells in blue (DAPI). The presence of non-neural cells indicates damage, and is notable in the vicinity of the largest non-splayed electrode bundle, and nearly absent around individual electrodes.

electrical contact with neurons, but we are more interested in the ability to record signals (see Section 3.2).

### 3.2 Chronic recording

#### Impedances

**HVC** Long-term recording in HVC is difficult due to skull regrowth interfering with electrodes implanted only a few hundred microns from the surface: after 10 months, we had difficulty picking up antidromic response in our two remaining birds.

**Area X** More telling of the potential of these electrodes is the recording of spontaneous activity in Area X, which was still easily seen in several channels after a year. Fig. 5 shows recordings in the weeks leading up to the 1-year mark. These are the three most stable electrodes of the 16.

### 3.3 Stimulation

**Minimising stimulation voltage** Some CSCs were better at triggering an antidromic response than others. From the  $2^{11}$  possible CSCs we chose 32 (30 randomly, and the two that treated all electrodes identically). For each CSC, we

Need a graph showing impedances per electrode over time. At least I have data for that; just haven't writtent the code to extract+plot.

I don't have recording-only data from early on.

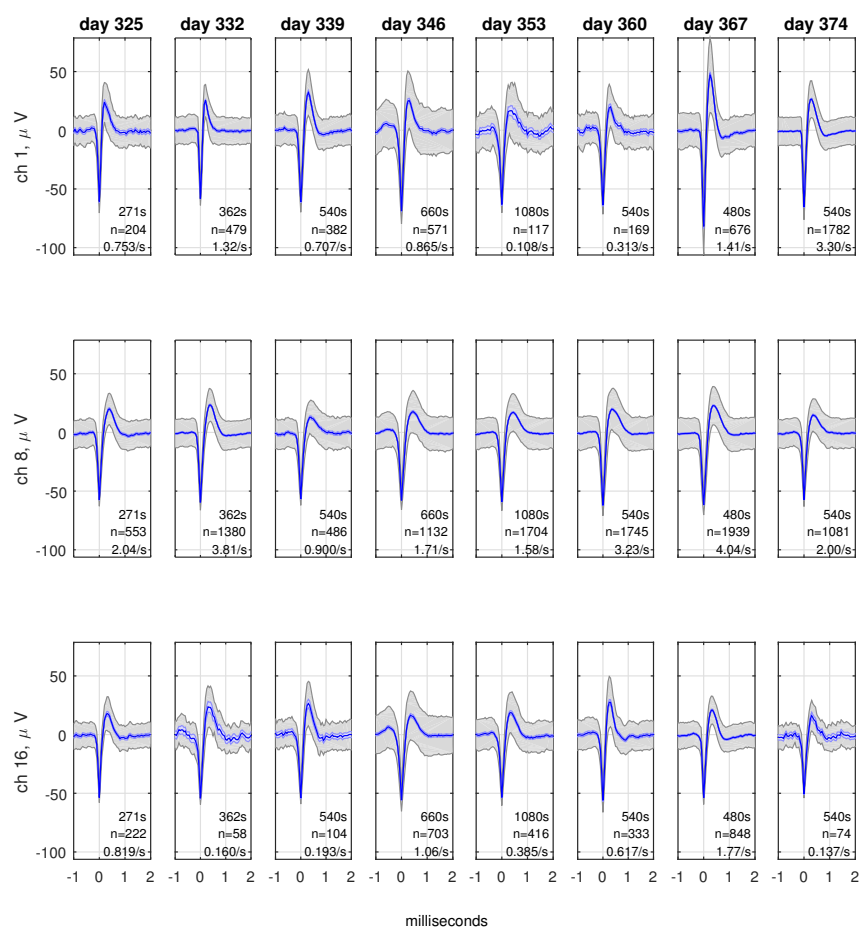


**Figure 5.** Some of the electrodes in Area X record spontaneous spikes a year after implantation. Column titles show the day post-surgery and the number of seconds of recorded data. Each row is one electrode (shown here: only the three most stable channels out of the 16). Legends show the number of seconds of the recording, the number of spikes, and mean spike rate. The grey shaded region is standard deviation, and the blue shaded region is the 95% confidence interval for the mean.



performed a threshold scan to find the minimum current needed to trigger a response. 284  
 When this current was found, we performed a voltage scan to find the maximum 285  
 potential on any electrode. We tested each CSC five times on an anaesthetised bird. 286  
 Results are shown in Fig. 6. The best CSCs resulted in a maximum voltage of around 287  
 1 V, while the worst were over 2.5 V. Perhaps surprisingly, the CSCs that sent 288  
 identical pulses to all 11 electrodes were among the worst performers, with our simple 289  
 search revealing CSCs that kept voltages far lower. 290

The maximum-likelihood fits to the voltage sweep data (green errorbars in Fig. 6) 291  
 consistently yield slightly higher threshold voltages than those measured using the 292  
 search. This is because whereas the maximum-likelihood fit computes the voltage 293  
 required in order to obtain a response with 50% probability, the threshold search, 294  
 which guided data acquisition in realtime, looks for any significant correlation between 295  
 the responses in each spike train, which is detectable well before the stimulation 296  
 achieves a 50% response rate. 297

## Controlling the antidromic response 298

# 4 Discussion 299

## 4.1 Steering 300

[13] showed good capacity to control stimulation by steering current between 301  
 electrodes in monkey retina, allowing targeting of neurons on a smaller scale than the 302  
 electrode spacing. The demonstration of fine control is compelling, but whether or not 303  
 the locally linear predictive response model that they found effective in retina would 304  
 be extensible to regions with greater lateral connectivity is unknown. 305

[24] showed that injecting current into tissue causes neurons whose axons are very 306  
 close to the stimulation site to fire, rather than neurons whose bodies are at greater 307  
 distances. As a result, the set of neurons that respond to a stimulation pulse is highly 308  
 sensitive to electrode location, but has spatial extent similar to that of the neuron's 309  
 dendritic tree. Furthermore, they showed that neurons stimulated in this manner 310  
 seldom stimulate downstream neurons synaptically. 311

Splaying electrode arrays with learning stimulation software may be able to exploit 312

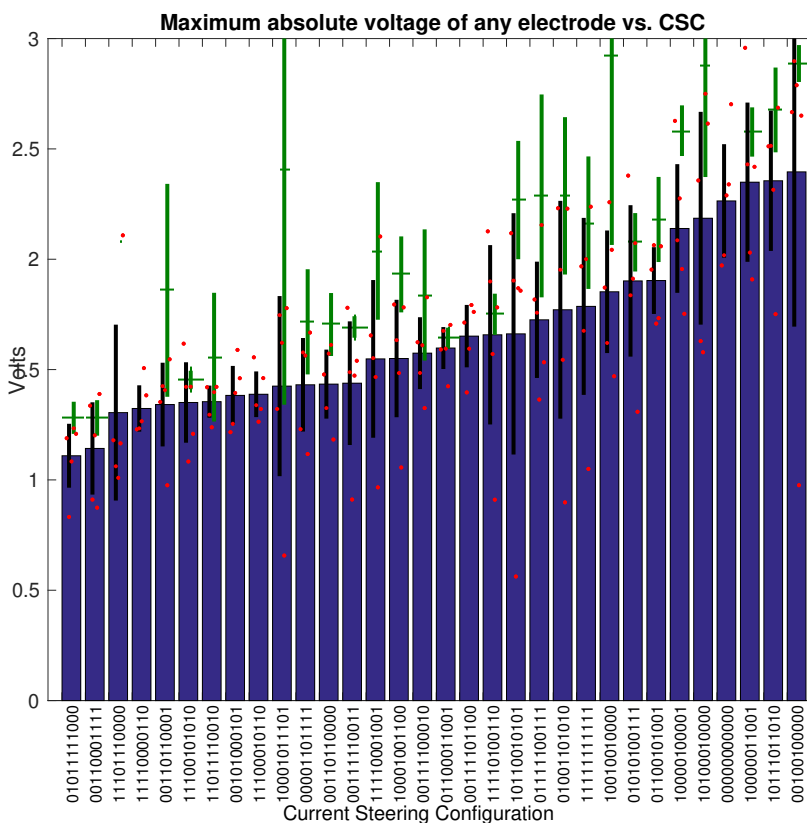


**Figure 6.** The peak Area X stimulation voltage required in order to achieve biologically effective levels of stimulation in HVC varies with different current-steering configurations. Here are 32 different configurations, over 5 trials each, taken 214 days post-surgery. The X axis lists the configuration (each of the 11 active electrodes delivers a positive-first “0” or negative-first “1” current-controlled pulse). The Y axis shows the maximum voltage across any electrode for the given CSC at the lowest current that evoked a reliable response. Red dots show the voltage results for each trial, and error bars are 95% confidence intervals ( $n=5$ ). Green bars show maximum-likelihood sigmoid fits for the voltage required to induce 50% probability of response using a completely separate analysis of the data (see Methods), also as 95% confidence intervals (when the lines would have spanned the whole range of the graph, they have been omitted for clarity), and with crossbar marker at the mean, with marker size chosen to give an approximate sense of confidence.

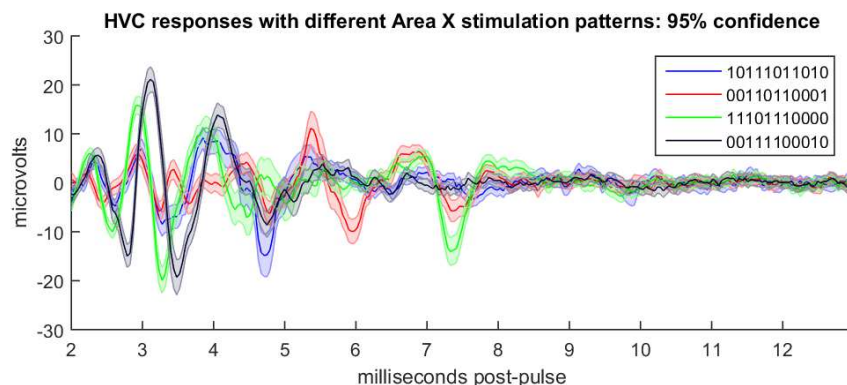


**Figure 7.** Different CSCs delivered to Area X can induce different responses antidromically in HVC. Here are four of the most distinct responses to four of the 32 CSCs shown in Fig. 6. Shading is 95% confidence,  $n=198$ .

these properties. First consider each of the  $n$  electrodes in our array separately.  $n$  sites stimulated at a given current gives  $n$  different random sets of  $k_n$  neurons that will fire, and increasing the current changes the size of  $k$ . There may exist multiple downstream neurons  $y$  such that directly-stimulatable neurons from several of our  $n$  sets synapse onto  $y$ . This creates a search problem: how to stimulate the  $n$  sets in a way that reliably stimulates  $y$  enough to cause it to spike? This requires search over current delivered to each group in  $n$  in order to control which neurons are recruited, and timing of stimulation delivery to each group in  $n$ , so that the downstream neuron is reliably triggered. Different values of current and timing delivered into the  $n$  groups may trigger different downstream neurons, so the search problem is: find as many different downstream neurons as possible.

Furthermore, it seems likely that directly-stimulatable neurons may synapse onto others that are directly-stimulatable, once or  $r$  times removed. This suggests a further dynamic for the timing search, in which different timings for stimulating the  $n$  sets may trigger different firing sequences ([13] proposes a related mechanism in the context of current steering in retina). This enlarges the space of inducible dynamics considerably, and suggests the possibility of inducing Hebbian learning.

Whereas Histed used single electrodes, we use multichannel arrays. Rather than a 16-channel array providing  $n = 16$  groups of neurons, different current-steering configurations may lead to a much higher value of  $n$ . For such an electrode there are  $2^{16}$  current-steering configurations even without manipulating current pulse magnitude or timing.

## 4.2 Ongoing Learning

Now where did I read this...?

The best clinical outcomes require about 20 hours of tuning time, involving multiple patient visits to a clinic.

## 4.3 Power

Another limitation of DBS systems is power use: even with on-demand therapy, the currents required in order to achieve good clinical outcome drain power fast. Small electrodes that drastically reduce scarring allow stimulation currents several orders of magnitude lower than state-of-the-art systems, and even if current steering does not allow realtime therapy optimisation, it appears to allow further optimisation of power usage.

## References

1. Butson CR, McIntyre CC. Current steering to control the volume of tissue activated during deep brain stimulation. *Brain Stimulation*. 2008;1:7–15. Available from: <http://www.sciencedirect.com/science/article/pii/S1935861X07000058>.
2. Barrese JC, Aceros J, Donoghue JP. Scanning electron microscopy of chronically implanted intracortical microelectrode arrays in non-human primates. *J Neural Eng*. 2016 April;13(2). Available from: <http://www.ncbi.nlm.nih.gov/pmc/articles/PMC4854331/>.
3. Biran R TP Martin DC. Neuronal cell loss accompanies the brain tissue response to chronically implanted silicon microelectrode arrays. *Experimental Neurology*. 2005 September;195(1):115–126. Available from: <http://www.ncbi.nlm.nih.gov/pubmed/16045910>.
4. VS P, PA T, WM R. Response of brain tissue to chronically implanted neural electrodes. *Journal of Neuroscience Methods*. 2005 October;148(1):1–18. Available from: <http://www.ncbi.nlm.nih.gov/pubmed/16198003>.

5. Winslow BD, Christensen MB, Yang WK, Solzbacher F, Tresco PA. A  
comparison of the tissue response to chronically implanted Parylene-C-coated  
and uncoated planar silicon microelectrode arrays in rat cortex. *Biomaterials*.  
2010 December;31(35):9163–9172. Available from:  
<http://www.sciencedirect.com/science/article/pii/S0142961210006873>.
6. Guitchounts G, Markowitz JE, Liberti WA, Gardner TJ. A carbon-fiber  
electrode array for long-term neural recording. *Journal of Neural Engineering*.  
2013;10(4). Available from:  
<http://www.ncbi.nlm.nih.gov/pmc/articles/PMC3875136/>.
7. Cogan SF. Neural Stimulation and Recording Electrodes. *Annual Review of*  
*Biomedical Engineering*. 2008;10(1):275–309. PMID: 18429704. Available from:  
<http://dx.doi.org/10.1146/annurev.bioeng.10.061807.160518>.
8. Udupa K, Chen R. The mechanisms of action of deep brain stimulation and  
ideas for the future development. *Progress in Neurobiology*. 2015;133:27–49.  
Available from:  
<http://www.sciencedirect.com/science/article/pii/S030100821500088X>.
9. Holloway KL, Gaede SE, Starr PA, Rosenow JM, Ramakrishnan V, Henderson  
JM. Frameless stereotaxy using bone fiducial markers for deep brain  
stimulation. *J Neurosurg*. 2005;103(3):404–413.
10. Chaturvedia A, Foutza TJ, McIntyre CC. Current steering to activate targeted  
neural pathways during deep brain stimulation of the subthalamic region. *Brain*  
*Stimulation*. 2012 July; Available from:  
<http://www.sciencedirect.com/science/article/pii/S1935861X11000672>.
11. Tuch DS, Wedeen VJ, Dale AM, George JS, Billiveau JW. Conductivity tensor  
mapping of the human brain using diffusion tensor MRI. *PNAS*. 2001  
September;98(20):11697–11701. Available from:  
<http://www.pnas.org/content/98/20/11697.full.pdf>.
12. Alexander AL, Lee JE, Lazar M, Field AS. Diffusion Tensor Imaging of the  
Brain. *Neurotherapeutics*. 2007 July;4(3):316–329. Available from:  
<http://www.ncbi.nlm.nih.gov/pmc/articles/PMC2041910/>.

13. Jepson LH, Hottowy P, Mathieson K, Gunning DE, Dabrowski W, Litke AM, et al. Spatially Patterned Electrical Stimulation to Enhance Resolution of Retinal Prostheses. *Journal of Neuroscience*. 2014 April;34(14):4871–4881. Available from: <http://www.jneurosci.org/content/34/14/4871.full>.
14. King JDH. Method for optimizing search for spinal cord stimulation parameter settings. Google Patents; 2006. US Patent 7,146,223. Available from: <https://www.google.com/patents/US7146223>.
15. Parramon J, Carbunaru R, Haller MI. Current steering for an implantable stimulator device involving fractionalized stimulation pulses. Google Patents; 2011. US Patent 7,890,182. Available from: <https://www.google.com/patents/US7890182>.
16. Priori A, Foffani G, Rossia L, Marceglia S. Adaptive deep brain stimulation (aDBS) controlled by local field potential oscillations. *Experimental Neurology*. 2013 July;245:77–86. Available from: <http://www.sciencedirect.com/science/article/pii/S0014488612003755>.
17. Afshar P, Khambhati A, Stanslaski S, Carlson D, Jensen R, Linde D, et al. A translational platform for prototyping closed-loop neuromodulation systems. *Frontiers in Neural Circuits*. 2012 January;6(112). Available from: <http://www.ncbi.nlm.nih.gov/pmc/articles/PMC3551193/>.
18. Priori A. Technology for Deep Brain Stimulation at a Gallop. *Movement Disorders*. 2015; Available from: <http://onlinelibrary.wiley.com/doi/10.1002/mds.26253/pdf>.
19. Rosin B, Slovik M, Mitelman R, Rivlin-Etzion M, Haber SN, Israel Z, et al. Closed-Loop Deep Brain Stimulation Is Superior in Ameliorating Parkinsonism. *Neuron*. 2011 October;72(2):370–384. Available from: <http://www.sciencedirect.com/science/article/pii/S0896627311007768>.
20. Long MA, Jin DZ, Fee MS. Support for a synaptic chain model of neuronal sequence generation. *Nature*. 2010 October;468(7322):394–399. Available from: <http://www.ncbi.nlm.nih.gov/pmc/articles/PMC2998755/>.

21. Hahnloser RHR, Kozhevnikov AA, Fee MS. An ultra-sparse code underlies the generation of neural sequences in a songbird. *Letters to Nature*. 2002 September;419:65–70. Available from: <http://www.nature.com/nature/journal/v419/n6902/full/nature00974.html>
22. Swadlow HA. Neocortical efferent neurons with very slowly conducting axons: strategies for reliable antidromic identification. *Journal of Neuroscience Methods*. 1998 February;79(2):131–141. Available from: <http://www.sciencedirect.com/science/article/pii/S0165027097001763#BIB51>
23. Fee MS, Kozhevnikov AA, Hahnloser RHR. Neural Mechanisms of Vocal Sequence Generation in the Songbird. *Ann NY Acad Sci*. 2004;1016:153–170. Available from: <http://web.mit.edu/feelab/publications/Fee%20et%20al%20NYAS%202004.pdf>
24. Histed MH, Bonin V, Reid RC. Direct activation of sparse, distributed populations of cortical neurons by electrical microstimulation. *Neuron*. 2009 August;63(4):508–522. Available from: <http://www.ncbi.nlm.nih.gov/pmc/articles/PMC2874753/>